LM-06K056
May 30, 2006

CFD Simulation of Flow Tones from Grazing Flow past a Deep Cavity

T Bagwell

NOTICE

This report was prepared as an account of work sponsored by the United States Government. Neither the United States, nor the United States Department of Energy, nor any of their employees, nor any of their contractors, subcontractors, or their employees, makes any warranty, express or implied, or assumes any legal liability or responsibility for the accuracy, completeness or usefulness of any information, apparatus, product or process disclosed, or represents that its use would not infringe privately owned rights.

Proceedings of IMECE06
2006 ASME International Mechanical Engineering Congress and Exposition
November 5-10, 2006, Chicago, Illinois USA

IMECE2006-15633

CFD SIMULATION OF FLOW TONES FROM GRAZING FLOW PAST A DEEP CAVITY

Ted G. Bagwell
Lockheed Martin
PO Box 1072
Schenectady, NY 12301

ABSTRACT

Locked-in flow tones due to shear flow over a deep cavity are investigated using Large Eddy Simulation (LES). An isentropic form of the compressible Navier-Stokes equations (pseudo-compressibility) is used to couple the vertical flow over the cavity mouth with the deep cavity resonances (1). Comparisons to published experimental data (2) show that the pseudo-compressible LES formulation is capable of predicting the feedforward excitation of the deep cavity resonator, as well as the feedback process from the resonator to the flow source. By systematically increasing the resonator damping level, it is shown that strong lock-in results in a more organized shear layer than is observed for the locked-out flow state. By comparison, weak interactions (non-locked-in) produce no change in the shear layer characteristics. This supports the 40 dB definition of lock-in defined in the experiment.

NOMENCLATURE

c	speed of sound
f	frequency
L	cavity streamwise length
L_c	cavity depth (vertical length)
L_z	cavity spanwise length
P_{ref}	reference pressure ($2X10^{-5}$ Pa)
Q	resonance quality factor
r	applied damping
S_{ij}	rate of strain tensor
u_i	velocity
U_o	free stream velocity
Δf	frequency resolution
Φ_n	pressure power spectrum
λ	spanwise integral length scale
ν	kinematic viscosity
ν_{SGS}	sub-grid scale eddy viscosity
θ	boundary layer momentum thickness at the cavity separation point
Δf	frequency resolution
$<u>$	time averaged velocity
u_{rms}	rms velocity

INTRODUCTION

Shear flow over a deep cavity (or quarter wave resonator) can generate strong, self-sustained flow oscillations. These cavity flow oscillations can couple into nearby acoustic resonators to produce noise. If the interaction of the flow oscillation and the acoustic resonance is weak, the flow source will not be influenced by the acoustic field and the resultant noise is typically small. However, if the interaction is strong enough, the acoustic perturbations will reinforce the flow oscillation producing even higher noise levels. This closed-loop phenomenon is referred to as flow tone lock-in. Flow tone lock-in can occur in a variety of configurations such as grazing flow over a Helmholtz resonator (1, 7), or a deep cavity, (2) and often produces excessively high noise levels. Lock-in can be mitigated using a variety of techniques, including increasing the acoustic resonator damping level.

Deciding whether or not an interaction is in fact "locked-in" can be a challenge, since direct flow source measurements are often not available. More likely, acoustic pressure measurements in or near the resonator are the only available observations. Given this, lock-in is often defined based on an arbitrary level of some parameter such as the Strength of Lock-in (SoL) (5). In the SoL approach, the amplitude of the acoustic resonance is tracked versus flow rate. SoL is then defined by the excess amplitude of the acoustic spectral peak over the background level produced by turbulence. The interaction is

Copyright © 2006 by ASME

considered to be locked-in if the SoL exceeds a predefined level.

Transient Computational Fluid Dynamics (CFD) techniques, such as Large Eddy Simulation (LES), have demonstrated success in characterizing noise sources, such as in open jets (8). In fact, fluid-resonant effects can be captured by compressible CFD simulations, as is demonstrated in the cavity-Helmholtz resonator configuration reported in Reference (1). As such, these methods should be suitable for examining lock-in potential and understanding how the flow source changes during lock-in.

In this paper, the lock-in due to grazing flow over a deep cavity will be investigated. The results will be verified by comparison to the test data in Reference (2). To examine the effect of lock-in on the flow source, the acoustic resonator damping level will be systematically increased to identify the onset of lock-in and the associated flow source changes. Furthermore, the receptivity of the cavity source to external acoustic waves will be investigated for comparison to test data.

SUMMARY OF THE LEHIGH EXPERIMENT

This section provides a summary of the test presented in Reference (2). Figure 1 illustrates the experimental apparatus. The rectangular side branch has a length, L, in the streamwise direction and the depth, L_C, in the vertical direction. Both the length and the depth were varied during the test. The cavity span was fixed at 1 inch. The test was conducted in air.

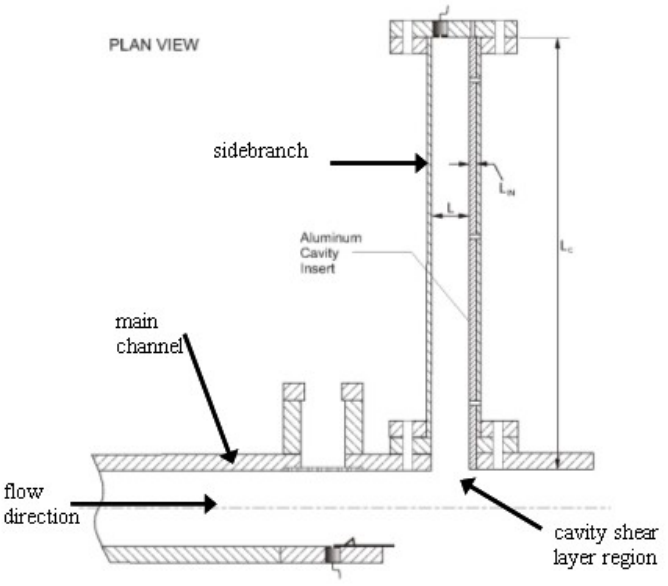

Figure 1. Schematic of deep cavity test.

The test reported on acoustic measurements with varying combinations of cavity length and depth. The individual cases have designations such as L2Lc19, which stands for a cavity length of 2 inches and a depth of 19 inches. For each cavity, the inlet velocity was systematically increased to map out the interaction of individual hydrodynamic modes with acoustic modes. Figure 2 shows a typical result, where the color contours refer to the log of pressure amplitude versus frequency. In these figures, major interactions have labels such as h1a3. This stands for the first hydrodynamic mode (h1) interacting with the third acoustic mode (a3). The hydrodynamic modes are the stages of cavity Strouhal numbers which scale roughly as,

$$St_n = \frac{fL}{U} \approx 0.6 * \left(n - 1/4\right), \qquad n = 1,2,3,4.. \tag{1}$$

This correlation fits the experimental data to within approximately 25% for the cases examined in this report. The acoustic modes (a1, etc.) of the side branch follow the relation:

$$f_m = \frac{mC}{4\left(L_C + \Delta\right)}, \qquad m = 1,3,5,... \tag{2}$$

$$\Delta = \text{end correction} \approx 1"$$

The end correction was determined based on the observed frequencies in the experiment.

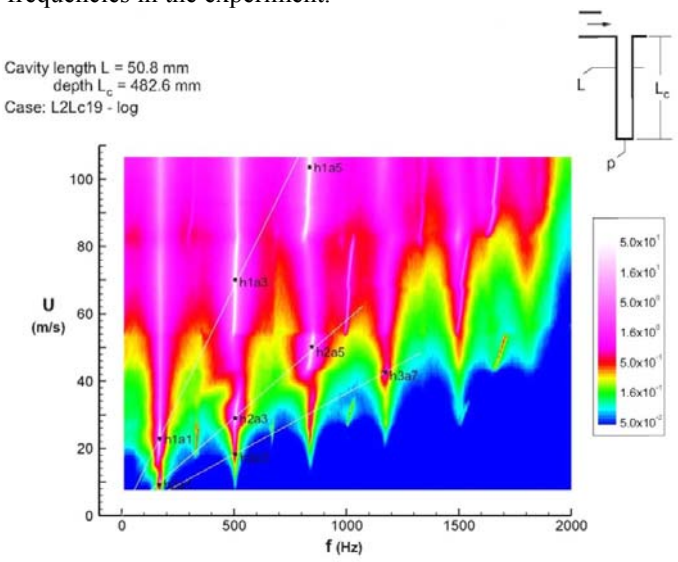

Figure 2. Plan view of pressure amplitude on a log scale as a function of frequency and velocity. From Figure 3.20b of Reference (2).

A criterion for characterization of flow tone lock-in is the strength of lock-in (SoL). SoL represents the excess amplitude of the (acoustic) spectral peak over the background level produced by turbulence. The procedure is described in detail in (5). In the Lehigh experiments, a SoL greater than 40 dB was used as the criteria for lock-in.

Copyright © 2006 by ASME

CFD MODEL FORMULATION

A base case was chosen to compare the experimental results against the CFD predictions. The base case corresponds to the Lehigh cavity case with a cavity length of 2 inches and a cavity depth of 19 inches (L2Lc19). The computational domain is shown in Figure 3. The cavity has a spanwise extent of 1 inch. As in the experiment, the incident boundary layer develops in a 1.5 inches tall open channel. The channel is open to a large acoustic expansion chamber, which was added to simulate radiation into a large three dimensional space. The origin of the coordinate system is the cavity leading edge at the half span location.

The boundary conditions on the model are also shown in Figure 3. The inflow condition was generated from an upstream simulation of a turbulent boundary layer flow, which will be described further in this report. The bottom wall of the main channel and all of the cavity walls were modeled as no-slip. The sidewalls (z normal) of the channel and cavity were modeled as free slip. The outflow surface was modeled with a fixed (natural) pressure boundary condition.

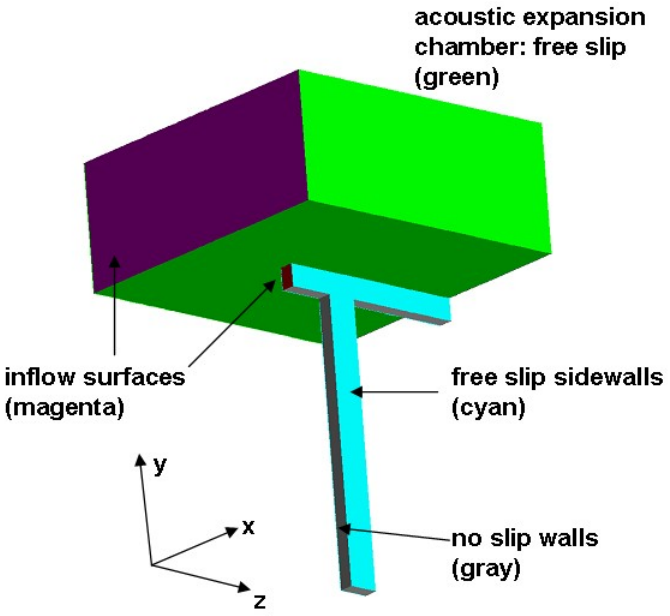

Figure 3. Schematic of the cavity configuration with boundary conditions indicated.

CFD COMPUTATIONAL FORMULATION

These simulations were performed using a commercially available finite element based flow solver known as ACUSOLVE. This code has been shown to yield excellent results for benchmark problems such as Tollmein-Schlicting wave propagation (ie. initial growth rate of turbulent inception), turbulent channel flow, turbulent pipe flow and laminar flow over a cylinder.

As in Reference (1), the pseudo-compressible form of the Navier-Stokes equations will be used. In this approach, a compressibility term is added to the incompressible conservation of mass equation:

$$\left(\frac{1}{\rho c^2}\right)\frac{\partial p}{\partial t}+\frac{\partial u_i}{\partial x_i}=0 \tag{3}$$

$$\frac{\partial u_i}{\partial t}+u_j\frac{\partial}{\partial x_j}u_i=-\frac{1}{\rho}\frac{\partial p}{\partial x_i}+\frac{\partial}{\partial x_j}\left(2(\nu+\nu_{SGS})S_{ij}\right)$$
$$-2r(u_i-\langle u_i\rangle)+F_i$$

ν_{SGS} = turbulent viscosity from the subgrid - scale model

$\langle u_i\rangle$ = time averaged velocity

This is an approximation to the fully compressible Navier-Stokes equations, where two approximations have been made:

- The effect of entropy waves has been neglected (ie. isentropic flow).
- The Mach number is small (and therefore convective effects on the acoustic waves have been ignored).

Past experience in Reference (1), indicates that this approach is valid for flows ranging in Mach Number from 0-0.1. To artificially dampen the resonator, the damping function, r, is applied to the momentum transport equations. This damping term is needed to simulate physical damping processes, such as wall compliance, which are not accounted for in the computations. The source term, F_i, will be used to simulate external excitation, such as from a loudspeaker.

The LES subgrid scale turbulence model employed in these calculations is a variant of the dynamic model described in Reference (6).

CFD GRID FORMULATION

The tetrahedral grid was generated using Fortran coding. A close-up of the grid is shown in Figure 4. Table 1 lists specific grid resolutions. This level of boundary layer grid refinement has been used in past LES pipe, channel flow and boundary layer calculations, and shows acceptable results.

Copyright © 2006 by ASME

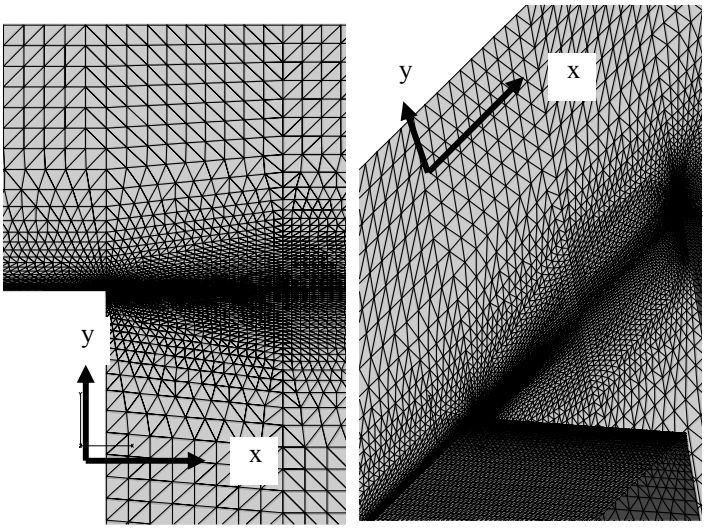

Figure 4. Cavity mesh.

	Domain Length (m)	Near wall mesh spacing (m)	near wall mesh spacing in wall units (based on u_τ = 1.17m/s)
Turbulent boundary layer streamwise (*x*)	0.0762	1.27 X10^{-3}	93
Turbulent boundary layer wall normal (*y*)	0.0381	2.54 X10^{-5}	1.9
Turbulent boundary layer and cavity spanwise (*z*)	0.0254	5.28 X10^{-4}	39
Cavity separation & impingement streamwise (*x*)	0.0508	1.27 X10^{-4}	10
Maximum cavity streamwise spacing	0.0508	1.27 X10^{-3}	93
cavity acoustic volume (isotropic in all directions)	0.4826	3.18 X10^{-3}	244

Table 1. Mesh parameters.

The timestep size was made proportional to the free stream velocity of the boundary layer:

$$\delta t = \frac{6.33X10^{-4}}{U_0(m/s)}s \tag{4}$$

In this way, the CFL[1] number in the center of the cavity was kept near 0.5. Unless otherwise noted, the simulations were run for 20,000 timesteps once a statistically steady flow was established. In real time, this corresponds to a total time record between 0.12 seconds and 0.7 seconds. While this time record is long enough to establish the long term behavior of the case, it is much shorter than the experimental time record size of 2 seconds. This implies that the frequency resolution of the CFD will be much coarser than the experiments.

TURBULENT BOUNDARY LAYER INFLOW GENERATION

An upstream simulation of a turbulent boundary layer was run to provide a fully turbulent inflow boundary condition for the cavity simulations. The grid for this calculation was extracted from the full cavity grid.

The boundary conditions on the case are as follows:

- A no slip wall boundary condition was employed at y = 0.
- The spanwise boundaries at z = +/- 0.0127 m are free slip. In the test, the sidewalls were un-tripped developing boundary layers. The difference is considered to be negligible because the sidewall boundary layers will be a very small part of the channel span and therefore will provide little damping to the turbulence in both the channel and the cavity.
- Natural pressure boundary conditions were employed at the high *x* and high *y* boundaries.
- The inflow velocity field was generated by a recycling technique similar to the one used by Lund, Wu & Squires (3). In this case, the turbulent velocity field at the recycle plane (*x* = 0.0508 m) is extracted at every timestep. The inflow velocity field at the next time is enforced via equation (4). Where $\theta^{recycle}$ is the computed momentum thickness at the recycle plane and θ^{inflow} is the specified momentum thickness at the inlet (0.483 mm). In effect, this boundary condition enforces a constant momentum thickness at the inflow plane. However, unlike Lund, Wu & Squires, this implementation does not preserve the correct relationship between the momentum thickness and the wall shear stress. For this boundary layer case, the free stream velocity was held at 36.6 m/s.

$$\underline{u}^{\inf low}(x,y,z) = \underline{u}^{recyclce}(x,\eta,z) \tag{5}$$
$$\eta = \frac{\theta^{\inf low}}{\theta^{recycle}} y$$

[1] Courant, Friedrichs and Lewy.

Copyright © 2006 by ASME

The resultant velocity profile at the recycle plane is shown in Figure 5. The final momentum thickness at the recycle plane was 0.54 mm, which is quite close to the empirical value of 0.56 mm. An artifact of the approximate recycling is that the wall shear stress is under-predicted. From theory, one would expect the skin friction coefficient to be, $C_f = 0.0256 * \mathrm{Re}_\theta^{-0.25} = 0.042$ (4), whereas the computation results in a skin friction coefficient of $C_f = 0.02$. This implies that the boundary layer in the simulation will grow too quickly downstream. However, it is believed that the most critical parameter for lock-in is the momentum thickness incident on the cavity (2). As the boundary layer thickness will be rescaled to match the experiments, the differences between the actual boundary layer and the approximate numerical boundary layer are considered to be negligible.

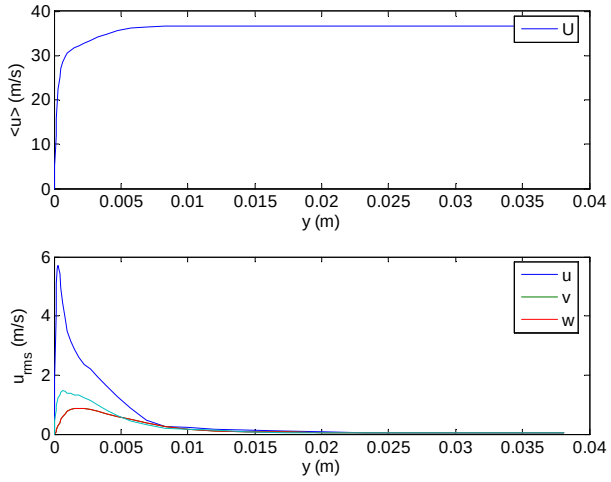

Figure 5. Mean and rms velocity profiles from the recycle plane.

The velocity field from the recycle plane was saved at every timestep for use as a boundary condition for the downstream cavity simulations. In order to apply the same boundary layer calculation for alternate flow points, the boundary layer data was rescaled using,

$$\underline{u}^{inflow}(x,y,z,t) = \frac{U_0}{36.6}\underline{u}^{recycle}(x,\eta,z,t) \quad (6)$$

$$\eta = \frac{\theta_{target}^{inflow}}{\theta^{recycle}} y$$

$$\theta_{target}^{inflow} = \frac{0.56 * \left(\frac{U_0}{36.6}\right)^{-0.2}}{1.21} (\mathrm{mm})$$

The 1.21 factor in the denominator was applied to account for the anticipated boundary layer growth from the inflow plane to the cavity leading edge.

ACOUSTIC RESONATOR CHARACTERIZATION

In order to show that the calculational setup has appropriate boundary conditions and numerics, a low flow resonator characterization was performed. In this case, the incident boundary layer velocity was replaced with a constant velocity of 0.37 m/s. At this flow rate, the velocity is low enough to prevent the cavity flow induced noise sources. The resonances were excited by applying a pulse of vertical momentum (an impact test) near y = -0.0254 m of the form:

$$F_2 = 0.001 * \exp(-\left[\frac{t - To}{\tau}\right]^2) \quad (7)$$

where

t = time

$To = 433\mu s$

$\tau = 104\mu s$

The linear damping term applied to this case is $2r$ = 66.97 rad/s, which results in a Q factor of 50 (1% critical damping) for the 505 Hz resonance. Damping was applied for y < -0.0254m. The damping amplitude was chosen to match the empirically determined values for the 505 Hz resonance. Simulations without this damping were found to have much larger Q factors than the experiment. Neither damping nor non-reflecting boundary conditions were required in the acoustic expansion chamber.

The timestep size used in this case was 17.3 μs. The simulation was run for 20,000 timesteps. Table 2 presents the resultant resonant frequencies and their corresponding quality factors, with comparison to the experimental data. The experimental quality factors are reproducible to within +/- 25%. The prediction of the resonant frequencies is quite good with less than 2 % error in comparison to experiment. This indicates that the calculation is capturing the acoustic frequencies of the deep cavity, including the end effect shift. The quality factors however, do not compare as well. The applied damping of $2r$ = 66.97 rad/s is the dominant dissipation mechanism in the cavity. As this value was chosen to match the empirical observation for the 505 Hz mode, the good agreement with the n=3 (a3) mode is to be expected. However, the applied damping is frequency independent, which results in a Q factor that is proportional to the frequency. This is the cause of the disagreement in the Q factors for the a1 & a5 modes.

mode #	resonant frequency (Hz)		quality factor	
	Exp.	LES	Exp.	LES

Copyright © 2006 by ASME

a1	167	166	47	19
a3	505	499	59	50
a5	844	831	57	78

Table 2. Resonator test resonant frequencies and quality factors.

FLOW SWEEP VALIDATION

In order to compare the simulated lock-in cases to experiment, a flow sweep was performed. Eight flow points were chosen between 18.3 m/s and 103 m/s, as shown in Table 3. At each flow point, the pressure at the base of the side branch was recorded to define the pressure power spectrum:

$$P_{rms} = \sum_{n=1}^{N} \Phi_n * \Delta f \tag{8}$$

$$\Phi_n(\mathrm{dB}) = 10 * \log_{10}(\Phi_n * \Delta f_{ref} / P_{ref}^2)$$

where,

$$\Delta f_{ref} = 1Hz$$

$$P_{ref} = 2X10^{-5} Pa$$

Figure 6 shows the response at each flow point with comparison to experiment. Several points may be made from the flow sweep comparison:

- At U = 18.3 m/s, the LES calculation correctly predicts the dominant h1a1 interaction (hydrodynamic mode 1 interacting with acoustic mode 1).
- At U = 27.45 m/s, the experiment exhibited substantial interactions at h1a1 and h2a3. In comparison, the LES predicts a stronger h2a3 interaction than the test. This may be due to the fact that acoustic mode 1 is overly damped in comparison to test.
- At U = 36.6 m/s, both the experiment and the LES exhibit weak interactions.
- At U = 50.14 m/s, the experiment observed a strong interaction at the h2a5 point. The LES calculation misses this feature. Instead, it predicts a stronger h1a3 interaction. The reason for this is uncertain. Given that the LES calculation has a higher Q for the 5th acoustic mode than the test; one would have expected that the LES would have been more likely to lock-in to the 5th mode. The other possibility is that the LES calculation has a weaker 2nd hydrodynamic mode than the test.
- At U = 54.9 m/s, both the LES and the experiment show a strong interaction at the h1a3 point.
- At U = 73.2 m/s, again, the dominant interaction point is h1a3. As in the experiment, this flow point is where the largest acoustic pressure was observed. A visualization of this interaction is provided in Figure 7.
- At U = 91.5 m/s, the experimental results show a strong interaction on the h1a5 point. While some h1a5 interaction is observed in the LES, the dominant response is still on the 3rd acoustic mode.
- At U = 103.6 m/s, both the LES and the experiment have fully transitioned to the h1a5 interaction point.
- For all flow points, the experiments exhibit broadband (feedforward only) excitation of the non-lock-in acoustic resonances. This feature is not as evident in the LES calculations. This is due to the short time window (coarse frequency resolution) of the calculations.

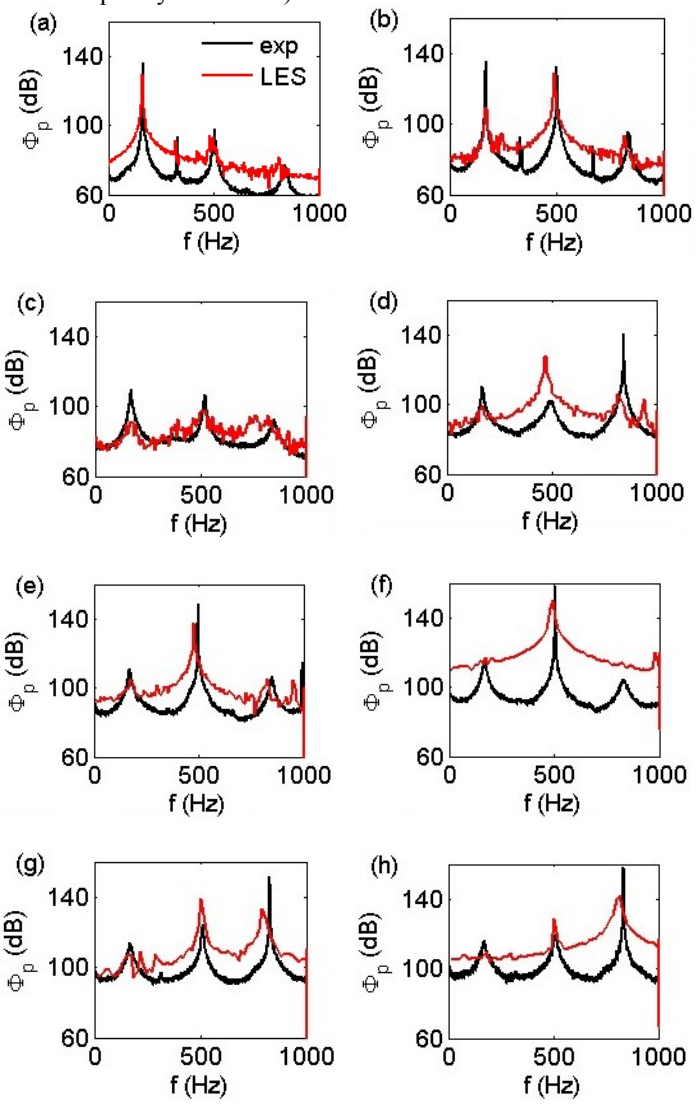

Figure 6. Flow sweep plots of side branch acoustic pressure power spectrum for flow points (a) U = 18.3 m/s, (b) U = 27.45 m/s, (c) U = 36.6 m/s, (d) U = 50.14 m/s, (e) U=54.9 m/s, (f) U=73.2 m/s, (g) U = 91.5 m/s & (h) U = 103.6 m/s.

The results in Figure 6 exhibit substantial agreement between test data and CFD. For points which do not compare well, the variability is most probably associated with differences in modal transition between the test and the LES. These differences are not well understood at present.

Copyright © 2006 by ASME

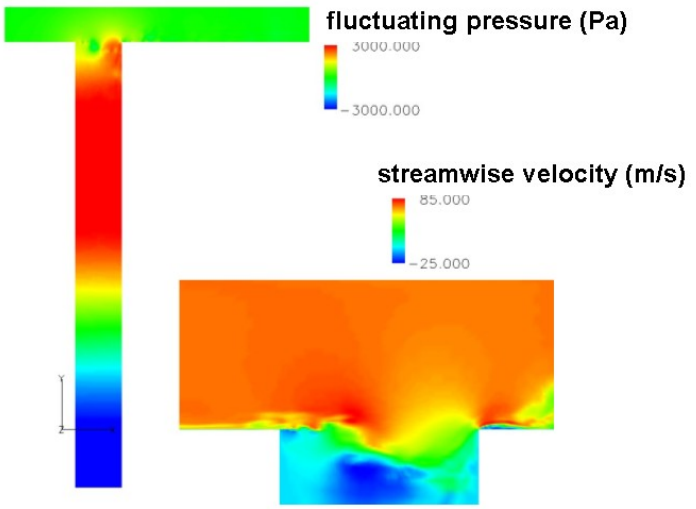

Figure 7. Visualization of the h1a3 interaction at U_o = 73.2 m/s.

The amplitude of the third acoustic mode as a function of flow rate is shown in Figure 8. This graph is generated by picking off the maximum pressure power spectrum values from Figure 6 for the a3 resonant peak. Figure 8 shows the dominant h1a3 (SoL=50 dB) and h2a3 (SoL = 46 dB) interactions reported in (2). The calculations are consistent with the experiments. However, unlike the experiments, the scarcity of velocity points in the calculations precludes the background level determination required by the SoL method. Alternate methods of determining lock-in will need to be used.

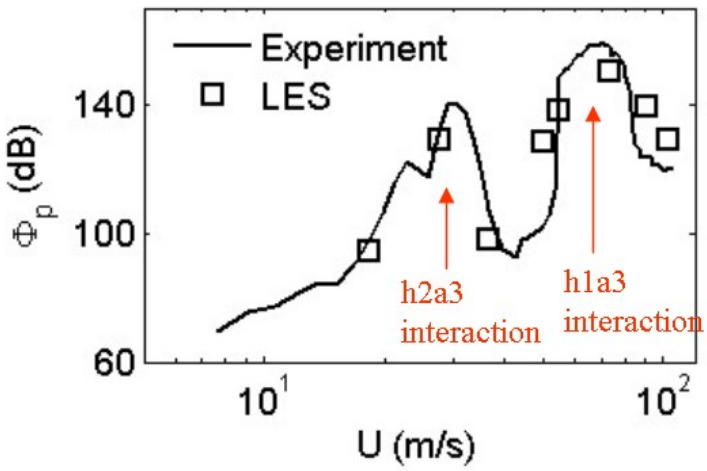

Figure 8. Variation of the third acoustic mode pressure amplitude as a function of flow rate

Previous analysis has suggested that the hydrodynamic stage is selected to match the most amplified shear layer mode at $f\theta/U_o$ = 0.017 (2). It is interesting to note that the h1a3 and h2a3 interactions shown in Figure 8 occurred for $f\theta/U_o$ < 0.005. Although this frequency is in the unstable range, linear stability theory suggests that higher frequencies are even more unstable, and therefore would be preferred for lock-in. This does not appear to be true here. For example, for the h1a3 interaction at U_o = 73.2 m/s, $f\theta/U_o$ = 0.004. Figure 2 shows that the 2nd hydrodynamic mode (h2) would have a frequency that is nearly coincident with the n=7 acoustic mode, which is a requirement for lock-in. At U_o = 73.2 m/s, the h2 stage would have a reduced frequency of $f\theta/U_o$ = 0.008. Using linear stability theory, one would estimate that the 2nd stage should be more unstable than the 1st stage. Given the frequency coincidence with the a7 acoustic mode and the presumably higher shear layer amplification for h2 hydrodynamic stage, one would have expected that an h2a7 interaction would have been preferred over the h1a3 interaction. Thus, it appears that factors other than linear stability theory are selecting the hydrodynamic stage.

In summary, the LES calculations do show trends which are physically consistent with the experimental lock-in observations. The major flow tone lock-in point at U_o = 73.2 m/s was predicted. The dominant h1 Strouhal source was able to excite the n=1, 3 and 5 acoustic modes at approximately the correct velocity. These calculations do show enough lock-in traits to be used to investigate factors which influence the lock-in cycle.

U_o (m/s)	Mode	Φ_p (dB)		frequency (Hz)	
		Exp	LES	Exp	LES
18.3	h1a1	136	129	164	161
27.5	h1a1	135	108	170	170
	h2a3	132	129	502	488
36.6	weak	109	91	174	170
	interaction	107	98	521	566
50.1	h1a3	102	128	499	470
	h2a5	140	106	846	817
54.9	h1a3	148	138	497	475
73.2	h1a3	158	150	506	490
91.5	h1a3	124	139	513	504
	h1a5	151	133	829	799
103.6	h1a3	120	129	514	506
	h1a5	158	142	835	807

Table 3. Summary of maximum excitation for flow points from the LES with comparison to experiment.

Copyright © 2006 by ASME

EFFECT OF INCREASED DAMPING

As mentioned in the previous section, defining lock-in via the SoL method using CFD is cost prohibitive because of the large number of flow points required. As an alternative, a series of increased acoustic damping runs was made, using the U=73.2 m/s flow point (h1a3 interaction) as a starting point. For these cases, it is more convenient to consider the pressure amplitude itself:

$$|P| = \sqrt{2\Delta f \Phi}$$
$$|P|(\mathrm{dB}) = 20\log_{10}(|P|/P_{ref}) \quad (9)$$

Starting from a least damped case (Q=100), the damping was sequentially increased to see where the case locks out. Figure 9 shows the resulting pressure amplitude measured at the base of the cavity. For the cases of Q=100, 50 and 25, the peak acoustic pressure amplitude was quite large and its amplitude is linearly proportional to the Q factor. When the damping was increased further to a Q=10, the amplitude drops by at least two orders of magnitude. This is a clear sign of non-linear behavior and indicates that the case locks out somewhere between Q=10 and Q=25.The results in Figure 9 can be used to estimate a lock-in inception point. If the case with Q=10 were to have followed the same (linear) trend as the higher quality factor cases, it would have had an acoustic pressure of approximately 159 dB and a peak acoustic particle displacement of 1.3 mm. Thus, for this case, it appears that a peak acoustic pressure of 159 dB is not strong enough to result in lock-in. Assuming that the calculations maintain the same turbulent background as the experiment, one would estimate that 159 dB corresponds to a SoL = 45. This value is quite close to the threshold of SoL=40 which was inferred in Reference (2).

Also, shown in Figure 9 is the peak acoustic particle displacement, which for the lock-in cases can be estimated from

$$|\varepsilon| = \frac{|p|}{\rho\omega c} \quad (10)$$

An interesting benchmark is that a peak acoustic particle displacement of 1.3 mm is almost twice the momentum thickness. From this, one would estimate that for lock-in to occur, the acoustic particle displacement needs to be on the order of the momentum thickness itself.

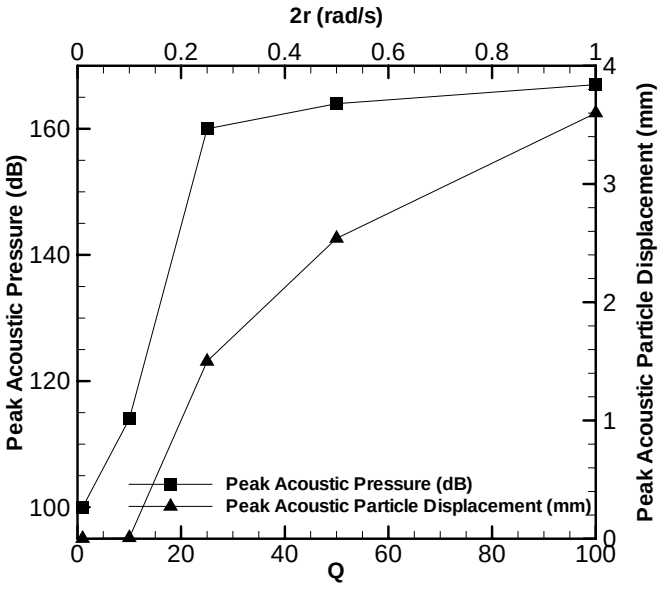

Figure 9. Acoustic pressure and particle displacement for varying damping factors.

Further evidence of the effect of lock-in on the flow source is given in Table 4, which shows the rms velocity levels and integral length scales.

$$R_i(z) = \frac{\langle u_i(x,y,z) * u_i(x,y,z=0) \rangle}{u_{i,rms}(x,y,z) * u_{i,rms}(x,y,z=0)} \quad (11)$$
$$\lambda_{zi} = \frac{1}{2}\int_{-L_z/2}^{L_z/2} R_i(z)dz$$

The spanwise rake was located in the streamwise center of the cavity (x=0.025m) at y=0 (near the center of the shear layer). For the non-lock-in cases, the streamwise rms velocity component dominates slightly and the wall normal and spanwise velocity components have nearly equal magnitude. The streamwise velocity is correlated for approximately 1/20th of the cavity span. The lock-in cases (Q>10) are substantially different. For the lock-in cases, the streamwise and vertical velocity components have nearly equal magnitude and are approximately 40% greater than the lock-out case. The spanwise velocity is 40% lower in the lock-in case as compared to the lock-out case. All three velocity components are well correlated across the span of the cavity for the lock-in case. This analysis shows that the flow source itself changes from a strongly three dimensional flow off of lock-in to a more two dimension flow field during lock-in. This is consistent with expectations.

Copyright © 2006 by ASME

Q factor	u_{rms}/U_o	v_{rms}/U_o	w_{rms}/U_o	λ_{z1}/L_z	λ_{z2}/L_z	λ_{z3}/L_z
1	0.18	0.15	0.14	0.04	0.14	0.07
10	0.18	0.15	0.14	0.04	0.14	0.07
25	0.23	0.24	0.09	0.38	0.42	0.1
50	0.22	0.31	0.09	0.40	0.46	0.14
100	0.23	0.40	0.08	0.43	0.48	0.17

Table 4. Summary of spanwise velocity statistics at x=0.0254, y=0.

CAVITY RECEPTIVITY TO ACOUSTIC PERTURBATIONS

The total lock-in cycle includes feedforward coupling, as well as feedback coupling. The feedforward coupling has a well defined theory. The feedback coupling does not. Feedback coupling is possible when the flow source changes in response to an external excitation (receptivity). This section will examine how receptive the cavity source oscillations are to externally imposed acoustic particle motions.

To analyze the receptivity, the cavity length was extended to L=45.6 inches in order to accommodate a larger damping region. Here, a source of momentum was applied at a y location corresponding to an acoustic pressure node:

$$F_2 = \begin{cases} A*\cos(2\pi*500*t)/6.35X10^{-3}\ (\mathrm{m/s^2}) \\ \quad for -12.75 < y < -12.5\ \mathrm{inches} \\ 0\ \mathrm{otherwise} \end{cases} \quad (12)$$

The resonances of the cavity were eliminated by increasing the damping from 66.97 rad/s to 6697 rad/second inside the cavity. By increasing the source amplitude, A, one can see where the source behavior begins to change.

Table 5 shows the rms velocity and spanwise correlation profiles for varying source amplitudes, A = 0, 0.34 m/s^2, 3.4 m/s^2, 17 m/s^2 and 34 m/s^2. The acoustic response with A = 0.34 m/ s and A = 3.4 m/s^2 are almost identical to the case with A=0, and therefore it is concluded that this level of acoustic forcing is incapable of changing the source. The case with A = 34 exhibits the same trends as the full lock-in case with strong correlation across the entire span of the cavity. The case with A = 17 is intermediate between these two distinct limits and thus represents the best estimate for receptivity inception. For this case, the maximum acoustic pressure amplitude was 666 Pa, which translates into an acoustic particle displacement of 0.52 mm, which is nearly equal to the momentum thickness itself.

This is consistent with the results observed in the increased damping case. Both studies imply that the cavity source is not easily influenced by external acoustic perturbations.

A (m/s^2)	u_{rms}/U_o	v_{rms}/U_o	w_{rms}/U_o	λ_{z1}/L_z	λ_{z2}/L_z	λ_{z3}/L_z
0	0.18	0.15	0.13	0.05	0.14	0.07
0.34	0.18	0.14	0.14	0.04	0.12	0.07
3.4	0.19	0.15	0.14	0.05	0.13	0.07
17	0.23	0.14	0.11	0.28	0.24	0.06
34	0.24	0.20	0.09	0.37	0.39	0.07

Table 5. Summary of spanwise velocity statistics at x=0.0254, y=0.

SUMMARY & CONCLUSIONS

This study represents the first attempt at validating computational lock-in against experiment. Overall, the results shown in Figure 6 compare very well to experiment. There is a general trend for lock-in to successively higher acoustic resonances with increasing flow. Lock-in interactions were observed for each of the first three hydrodynamic sources. For the strong h1a3 interaction in the L2Lc19 cavity, there is a clear change in the source behavior, which demonstrates that feedback from the resonator has changed the source. This demonstrates that lock-in behavior can be achieved numerically.

Lock-in behavior in the calculations was evaluated based on spanwise changes in the source behavior. Direct confirmation that feedback has occurred is characterized by increased integral length scale and reduced spanwise velocity, both of which indicate stronger two dimensional instability modes and suppression of three dimensional turbulence. By comparison, experiments infer lock-in based on increased resonator response, through the strength of lock-in. The inception point for lock-in, as judged by changes in the spanwise integral length scale, compare well to the inception point deduced from the strength of lock-in method. For future experiments, spanwise measurements would be valuable for direct confirmation of lock-in.

Some significant issues still need to be addressed. In the L2Lc19 case, the computation predicted an h1a5 interaction at U=50.1 m/s, whereas the test produced an h2a3 interaction. While the reason for this is unclear at present, it may be due to inadequacies in the applied damping or numerical damping of the higher cavity stages. An important challenge of computational lock-in is the ability to reproduce experimentally observed resonant behavior. In many cases, the damping is proportional to the square root of frequency or frequency to the first power (as is approximately the case for the Lehigh cavity). This behavior is difficult to reproduce in a time based CFD simulation, where the only easily applied damping is proportional to even powers of frequency (f^0,f^2, etc.). In addition, appropriate and realistic boundary conditions are required on both the incident velocity field as well as the acoustic field.

The cavity tends to have hydrodynamic-acoustic mode interactions at very small values of free shear layer Strouhal

Copyright © 2006 by ASME

numbers, even though hydrodynamic-acoustic mode interactions are available at frequencies which are much closer to the maximum amplified free shear layer instability. This indicates that, in addition to free shear layer instability, there are other factors which dictate the preferred interaction.

Both the increased damping and cavity receptivity studies suggests that acoustic particle displacement must be nearly equal to the momentum thickness itself in order to attain the feedback necessary to complete the lock-in cycle. This corresponds directly to a Strength of Lock-in of approximately 45 dB required for lock-in, which supports the empirical estimate of 40 dB.

ACKNOWLEDGMENTS

The computational grid generator was provided by Prof. K.E. Jansen (Rensselaer Polytechnic Institute). Prof. D.O. Rockwell (Lehigh University) was invaluable both for discussions and providing the empirical data. The author also acknowledges the helpful discussions with K. Lai Fook-Cody, S.P. Antal and D.A. Corson (Lockheed Martin).

REFERENCES

1. Inagaki, M., Murata, O., Kondoh, T., Abe, K., "Numerical Prediction of Fluid-Resonant Oscillation at Low Mach Number", AIAA Journal, Vol. 40, 2002.
2. Yang, Y. 2005 "Generation of Tones Due to Grazing Shear Flow Past a Deep Cavity", Ph.D. Thesis, Lehigh University.
3. Lund, T. S., Wu, X. & Squires, K. D. 1998 Generation of Turbulent Inflow Data for Spatially Developing Boundary Layer Simulations. Journal of Computational Physics. Vol. 140. pg. 233.
4. Schlicting, H. 1979 *Boundary Layer Theory*. McGraw-Hill.
5. Mendelson, R. S. 2003 "Methods of Measuring Lock-in Strength and Their Application to the Case of Flow over a Cavity Locking into a Single Side Branch", AIAA Paper 2003-3106.
6. Jansen, K.E. 1999 "A Stabilized Finite Element Method for Computing Turbulence". Computer Methods in Applied Mechanics and Engineering. Vol. 174. pp. 299-317.
7. Henderson, B.S. 2004. Sound Generation by Flow over a Cavity. in the *Fourth Computational Aeroacoustics (CAA) Workshop on BenchMark Problems*. NASA/CP-2004-212954.
8. Bogey, C. & Bailly, C. 2003. LES of a High Reynolds, High Subsonic Jet: Effects of the Inflow Condition on Flow and Noise. AIAA paper 2003-3170.

Copyright © 2006 by ASME